PCCP

ROYAL SOCIETY OF CHEMISTRY

PAPER

View Article Online
View Journal

Cite this: DOI: 10.1039/d5cp04719f

Observation of quasi-planar boron carbonyl complexes $B_{36}(CO)_n^+$ (n = 1–6) analogous to coronene monocation $C_{24}H_{12}^+$

Hong Niu, Qiang Chen,* Qin-Wei Zhang, Xi Chen, Teng Li, Xiao-Ni Zhao and Si-Dian Li*

The discovery of quasi-planar C_{6v} B_{36} and C_{2v} B_{36}^- (Piazza *et al., Nat. Commun.*, 2014, **5**, 3113) provided the first experimental evidence for the viability of 2D borophene nanomaterials. Joint chemisorption experiment and first-principles theory investigations conducted herein indicate that, as the well-defined global minimum of the monocation, geometrically similar to C_{6v} B_{36} and C_{2v} B_{36}^-, the size-selected quasi-planar C_{2v} B_{36}^+ (**1**) with six approximately equivalent tri-coordinate vertex B atoms can consecutively chemisorb up to six CO molecules under ambient conditions to form a series of quasi-planar $B_{36}(CO)_n^+$ analogous to coronene monocation C_{2h} $C_{24}H_{12}^+$ in π-bonding, presenting the largest boron carbonyl aromatics (BCAs) observed to date. Kinetic studies have demonstrated that quasi-planar C_{2v} B_{36}^+ is about 10, 100, and 1000 times less reactive in experiments towards the first CO than the previously reported perfect planar C_{2v} B_{13}^+, double-ring tubular D_{2d} B_{20}^+, and quasi-planar C_s B_{11}^+ and C_{2v} B_{15}^+, respectively. Extensive theoretical calculations and analyses revealed the chemisorption pathways and bonding patterns of the experimentally observed $B_{36}(CO)_n^+$ and their neutral counterparts $B_{36}(CO)_n$ (n = 1–6), which appear to possess two concentric delocalized π systems over the molecular plane analogous to that of coronene monocation C_{2h} $C_{24}H_{12}^+$ (6π©5π) and neutral coronene D_{6h} $C_{24}H_{12}$ (6π©6π), respectively, imparting dual π-aromaticity and high stability to the systems.

Received 4th December 2025,
Accepted 14th January 2026

DOI: 10.1039/d5cp04719f

rsc.li/pccp

Introduction

Carbon monoxide (CO), as a typical σ-donor, is one of the most important ligands in chemistry and catalysis.[1–3] In typical transition metal (TM) carbonyl complexes, CO donates its σ-lone pair on carbon (:C≡O) to the partially occupied (n−1)d orbitals of the TM center to form an effective σ-donation bond, whereas its two equivalent π* antibonding orbitals accept partial TM (n−1)d electrons to form two weak π-backdonation interactions perpendicular to each other. Recently, main group metal carbonyl complexes, such as $M(CO)_8$ (M = Ca, Sr, Ba), have also been discovered in experiments, suggesting that alkaline-earth metals can serve as "honorary transition metals" in carbonyl complexes.[4]

As a prototypical electron-deficient element in the periodic table, boron ([He]$2s^2 2p^1$) can form various types of carbonyl complexes. The closed-shell carbonyl borane H_3BCO[5] and its derivatives are experimentally known as stable boron carbonyl complexes. In recent years, various small boron carbonyl clusters, including linear BCO,[6] OCBBCO,[7] and BBCO;[8] V-shaped $B(CO)_2$,[9] rhombic $B_4(CO)_2$[10] and $B_4(CO)_3$;[11] and planar (2D) $B(CO)_3^+$, $B(CO)_4^+$, $B_2(CO)_4^+$, and $B_3(CO)_n^+$ (n = 3–6), have been observed in experiments *via* infrared photodissociation (IRPD) spectroscopy.[12–15] In these boron carbonyl complexes,: CO ligands serve as σ-donors to coordinate the B_n centers as σ-acceptors. Based on joint gas-phase mass spectroscopy, collision-induced dissociation (CID), and first-principles theory investigations, our group discovered in 2024 the first quasi-planar boron carbonyl aromatics (BCAs) $B_{13}(CO)_n^+$ (n = 1–7) analogous to benzene.[16] Subsequent studies in 2025 revealed the existence of quasi-planar $B_{11}(CO)_n^+$ (n = 1–6) and $B_{15}(CO)_n^+$ (n = 1–5) with π and σ conflicting aromaticity[17] and double-ring tubular $B_{20}(CO)_n^+$ (n = 1–8) with tubular aromaticity.[18] Quasi-planar C_{2v} B_{36}^- monoanion (C_{2v} [B_6©B_{12}©B_{18}]$^-$) and neutral C_{6v} B_{36} (C_{6v} [B_6©B_{12}©B_{18}]), which consist of three concentric rings with six approximately equivalent periphery tri-coordinate vertex B atoms at six corners, were discovered in 2014 in a joint photoelectron spectroscopy and first-principles theory investigation, presenting the first experimental evidence for the viability of 2D borophene nanomaterials.[19] The perfect bowl-shaped quasi-planar C_{6v} B_{36} proves to be the well-defined global

Institute of Molecular Science, Shanxi University, Taiyuan 030006, P. R. China. E-mail: chenqiang@sxu.edu.cn, lisidian@sxu.edu.cn

minimum of the neutral lying about 0.87 eV more stable than the second lowest-lying triple-ring-tubular isomer C_s B_{36}.[19] Chemical bonding analyses revealed that both neutral C_{6v} B_{36} and C_{2v} B_{36}^- monoanion are all-boron analogues of coronene ($C_{24}H_{12}$), featuring concentric dual π-aromaticity with an inner π-sextet and an outer π-sextet (6π©6π).[19,20] However, their monocation B_{36}^+ and its carbonyl complexes $B_{36}(CO)_n^+$ still remain unexplored in either experiments or theory to date, leaving critical gaps regarding the structural integrity between B_{36}, B_{36}^-, and B_{36}^+ and the influence of concentric dual π-aromaticity on CO coordination reactivity.

Based on extensive joint chemisorption experiment and first-principles theory investigations, we herein report the observation of a series of quasi-planar boron carbonyl complexes $B_{36}(CO)_n^+$ (n = 1–6) analogous to coronene monocation $C_{24}H_{12}^+$ in π-bonding. As the well-defined global minimum of the monocation, geometrically similar to C_{6v} B_{36} and C_{2v} B_{36}^-, the size-selected quasi-planar C_{2v} B_{36}^+ (**1**) (C_{2v} $[B_6©B_{12}©B_{18}]^+$) was found to be capable of chemisorbing up to six CO molecules consecutively under ambient conditions at the external vertices to form a series of quasi-planar $B_{36}(CO)_n^+$ monocations, presenting the largest BCAs reported to date. The experimentally observed $B_{36}(CO)_n^+$ and their neutral counterparts $B_{36}(CO)_n$ (n = 1–6) feature two concentric delocalized π systems over the molecular plane analogous to that of the coronene monocation C_{2h} $C_{24}H_{12}^+$ (6π©5π) and its neutral counterpart D_{6h} $C_{24}H_{12}$ (6π©6π), respectively.

Methods

Experimental methods

The experiments were conducted using a homemade reflection time-of-flight mass spectrometer (TOF-MS)[21–23] equipped with a laser ablation cluster source, a quadrupole mass filter (QMF),[24] and a linear ion trap (LIT)[25] reactor. Boron cluster monocations (B_n^+) were produced *via* laser ablation of a rotating and translating ^{11}B target (99% enriched) in an 8-atm He carrier gas atmosphere. The ablation was performed using a 532-nm pulsed laser (Nd^{3+}:YAG second harmonic) operating at a 10-Hz repetition rate with a pulse energy of 8 mJ. The B_{36}^+ monocations generated from the cluster source were mass-selected using the QMF and subsequently injected into the LIT reactor. Within the LIT, the cluster monocations were first confined and thermalized through collisions with 0.5-Pa He gas for about 5 ms and then allowed to interact with a pulse of CO reactant gas at room temperature. Following the reactions, the cluster ions were ejected from the LIT reactor and subsequently detected *via* TOF-MS.

The pseudo-first-order rate constants (k_1) for the reactions between B_{36}^+ clusters and CO were derived using the following equation:

$$\ln\frac{I_R}{I_T} = -k_1\frac{P_{effective}}{k_B T}t_R \quad (1)$$

where I_R denotes the signal intensity of the reactant cluster ions after reaction; I_T, the total ion intensity including contributions from product ions; $P_{effective}$, the effective pressure of the reactant gas in the ion trap reactor; k_B, the Boltzmann constant; T, the temperature (~300 K); and t_R, the reaction time. Further details regarding the derivation of k_1 can be found in ref. 26.

Theoretical methods

Using the Tsinghua Global Minimum (TGmin) program[27] based on the basin-hopping algorithm in conjunction with manual structural constructions derived from literature,[19,20] we performed extensive global-minimum searches on B_{36}^+, with over 7000 stationary points probed on the potential energy surface. Full structural optimizations were performed on the low-lying isomers using the Gaussian 16 program[28] at PBE0-D3/6-311+G(d) level,[29–31] which has proven to be reliable for describing the reactions of pure boron clusters with small molecules.[18,23] More accurate single-point calculations were performed on the most favourable chemisorption pathways of the experimentally observed $B_{36}(CO)_n^+$ (n = 1–6) using the high-level domain-based local pair natural orbital coupled cluster approach with single and double excitations and perturbative triples corrections [DLPNO-CCSD(T)][32] implemented in the ORCA program,[33] with the basis set of cc-pvtz for B, C, and O.[34,35] As expected, with one valence-electron detached, the open-shell quasi-planar C_{2v} B_{36}^+ (**1**, $^2\mathbf{A_1}$) proves to be the well-defined global minimum of the monocation consisting of three concentric rings (C_{2v} $[B_6©B_{12}©B_{18}]^+$) with six approximately equivalent tri-coordinate vertex B atoms at six corners on the outer B_{18} ring, slightly distorted from the well-established perfect bowl-shaped neutral C_{6v} B_{36} (C_{6v} $[B_6©B_{12}©B_{18}]$).[19] C_{2v} B_{36}^+ (**1**) turned out to be much more stable (by 1.17 eV) than the second lowest-lying triple-ring tubular isomer C_s B_{36}^+ in thermodynamics at the DLPNO-CCSD(T) level (Fig. S1), similar to the situation in neutral C_{6v} B_{36}, which lies about 0.87 eV more stable than its triple-ring tubular isomer C_s B_{36}.[19] In comparison, as the only isomer observed in ion-mobility experiments, the double-ring tubular S_4 B_{20}^+ monocation lies about 1.09 eV more stable than its second lowest-lying quasi-planar isomer C_s B_{20}^+.[36] We believe that C_{2v} B_{36}^+ (**1**) is most likely the only isomer observed in gas-phase experiments in which no inert isomers are observed when the reaction time is long enough (Fig. 1(a5)), although there is no measured IR-PD spectrum or ion-mobility experimental data available to confirm it. Previous CID experiments on $B_{13}(CO)_n^+$ complexes indicate that CO ligands are molecularly coordinated to boron cluster cores along the outer ring without activation or dissociation.[16] $B_{36}(CO)_n^+$ complexes were therefore constructed by coordinating n CO ligands around the quasi-planar B_{36}^+ (**1**) core along the outer B_{18} ring, with the six tri-coordinate vertex atoms at the six corners proving to be the most active coordination sites. Vibrational frequency analyses confirmed that all the optimized intermediates (IMs) and transition states (TSs) are genuine minima and first-order saddle points on the potential energy surfaces, respectively. Intrinsic reaction coordinate (IRC) calculations[37,38] verified that each TS connects two appropriate IMs (Fig. S7–S19). The potential energy surfaces for CO approaching $B_{36}(CO)_{n-1}^{+/0}$

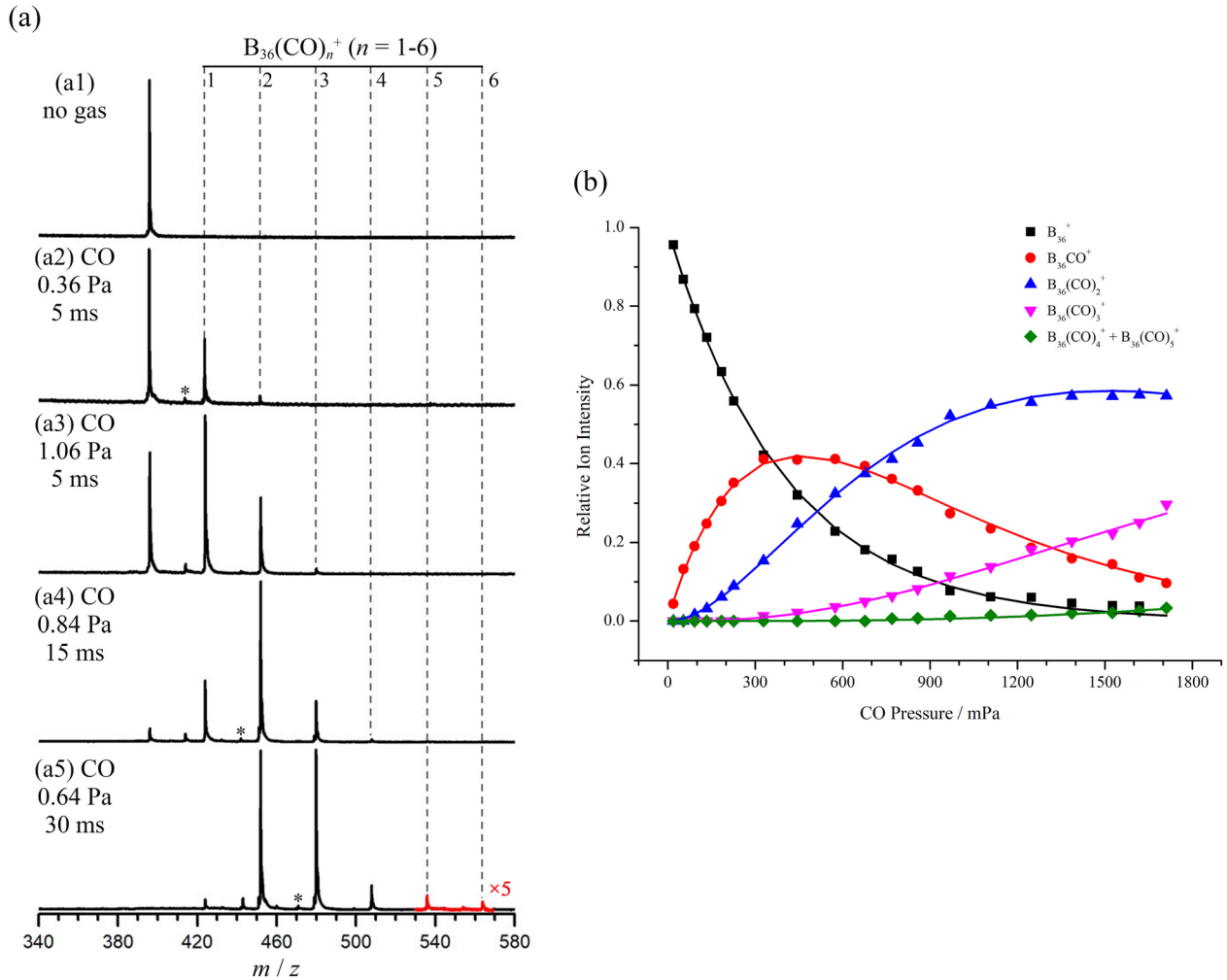

Fig. 1 (a) Measured TOF mass spectra for the reaction of mass-selected B_{36}^+ with CO, with the mass intensities between m/z = 530–570 in (a5) enhanced by five times. The CO reactant gas pressures and reaction times are indicated in Pa and ms, respectively. The weak mass signals marked with asterisks in a2, a4, and a5 can be assigned to $B_{36}(H_2O)^+$, $B_{36}(CO)(H_2O)^+$, and $B_{36}(CO)_2(H_2O)^+$, respectively, which arise from the existence of trace water impurities in the reaction system [$B_{36}(CO)_n^+ + H_2O \rightarrow B_{36}(CO)_n(H_2O)^+$ (n = 0–2)]. (b) Variation of the measured relative signal intensities of the reactant and product ions with respect to the effective reactant gas pressures in the reactions of $B_{36}^+ + nCO \rightarrow B_{36}(CO)_n^+$ (n = 0–6). The solid lines are fitted to experimental data points with the approximation of pseudo-first-order reaction mechanisms. Combined signal intensities of $B_{36}(CO)_4^+$ and $B_{36}(CO)_5^+$ are plotted in green diamonds.

were obtained through relaxed scans along the B–CO coordination distances.

Detailed chemical bonding analyses were conducted on the most concerned species using the adaptive natural density partitioning (AdNDP) approach.[39,40] The aromatic character was assessed by computing iso-chemical shielding surfaces (ICSSs) employing the Multiwfn 3.8 program[41] visualized using the VMD 1.9.3 software.[42] The gauge including magnetically induced current (GIMIC) method[43] was employed to calculate ring current densities and directions under a magnetic field perpendicular to the molecular planes. The resulting current densities were visualized using ParaView.[44] Energy decomposition analyses with natural orbitals for chemical valence (EDA-NOCV) approach[45–47] were conducted to analyse the coordination interactions in $B_{36}CO^+$ and $B_{36}CO$ at the PBE0/TZ2P level using the ADF (2023) program[48] with the zeroth-order regular approximation (ZORA).[49]

Results and discussion

Chemisorption experiments

The TOF mass spectra for the reactions of mass-selected B_{36}^+ cluster cations with CO at room temperature are collectively shown in Fig. 1(a). When B_{36}^+ was allowed to react with 0.36-Pa CO for 5 ms (Fig. 1(a2)), the first product $B_{36}CO^+$ was generated with a notable intensity, accompanied by a weak signal of $B_{36}(CO)_2^+$, whereas the reactant B_{36}^+ signal remained relatively strong. Increasing the CO pressure to 1.06 Pa (Fig. 1(a3)), the intensities of $B_{36}CO^+$ and $B_{36}(CO)_2^+$ were significantly enhanced, and a new product peak corresponding to $B_{36}(CO)_3^+$ distinctly emerged. Further increasing the reaction time to 15 ms with CO pressure of 0.84 Pa (Fig. 1(a4)), the B_{36}^+ signal was significantly reduced, the $B_{36}(CO)_2^+$ signal became dominant, and the weak signal of $B_{36}(CO)_4^+$ appeared. When the reaction

time was extended to 30 ms with a CO pressure of 0.64 Pa (Fig. 1(a5)), the reactant B_{36}^+ signal completely disappeared, whereas the relative intensities of $B_{36}(CO)_3^+$ and $B_{36}(CO)_4^+$ significantly increased. Relatively weak signals of $B_{36}(CO)_5^+$ and $B_{36}(CO)_6^+$ were also observed in Fig. 1(a5). No mass signals beyond $B_{36}(CO)_6^+$ were detected even under higher CO pressures or with prolonged reaction times. These experimental results indicate that B_{36}^+ can consecutively chemisorb up to six CO molecules under ambient conditions in the following reaction:

$$B_{36}^+ + nCO \rightarrow B_{36}(CO)_n^+ \ (n = 1\text{–}6) \qquad (2)$$

Based on a least-squares fitting procedure (Fig. 1(b)), the pseudo-first-order rate constants (k_1) for the reactions of $B_{36}(CO)_n^+$ (n = 0, 1, 2) with CO were estimated to be k_1 = 6.87×10^{-13}, 5.21×10^{-13}, and 1.26×10^{-13} cm^3 molecule^{-1} s^{-1} for n = 0, 1, and 2, with the corresponding reaction efficiencies of Φ = 0.11%, 0.08%, and 0.02%, respectively. Due to the relatively weak intensities of $B_{36}(CO)_4^+$ and $B_{36}(CO)_5^+$ in the mass spectra, their combined rate constant was estimated to be $k_1 = 4.92 \times 10^{-14}$ cm^3 molecule^{-1} s^{-1} [Φ = 0.01%] (Fig. 1(b), green diamonds). The estimated reaction rate constant k_1 of B_{36}^+ turned out to be about 10, 100, and 1000 times smaller than that of the quasi-planar B_{13}^+ ($k_1 = 4.26 \times 10^{-12}$ cm^3 molecule^{-1} s^{-1}) with typical π-aromaticity,[16] double-ring tubular B_{20}^+ ($k_1 = 2.65 \times 10^{-11}$ cm^3 molecule^{-1} s^{-1}) with tubular aromaticity,[18] and quasi-planar B_{11}^+ ($k_1 = 2.43 \times 10^{-10}$ cm^3 molecule^{-1} s^{-1}) and B_{15}^+ ($k_1 = 1.30 \times 10^{-10}$ cm^3 molecule^{-1} s^{-1}) with σ and π conflicting aromaticity,[17] respectively. Such a k_1 variation trend occurs possibly due to two reasons: (1) B_{36}^+ (**1**) possesses dual concentric π-aromaticity to effectively help stabilize the monocation, as will be discussed in detail later, and (2) the peripheral B atoms in B_{36}^+ (**1**) are less electron-deficient in average than that in the much smaller monocations, such as B_{11}^+, B_{13}^+, B_{15}^+, and B_{20}^+.

Chemisorption pathway analyses

Utilizing the quasi-planar B_{36}^+ (**1**) discussed above as coordination center and n CO molecules as ligands around it, the optimized lowest-lying structures of $B_{36}(CO)_n^+$ (n = 1–6) monocations and the corresponding most favorable chemisorption pathways are collectively shown in Fig. 2(a), with relative energies and energy barriers indicated at the single-point DLPNO-CCSD(T) level. Alternative low-lying isomers are depicted in Fig. S2–S6 at PBE0-D3/6-311+G(d). As shown in Fig. 2(a), the first CO ligand is coordinated to one of the six tri-coordinate vertex sites at the six corners of the quasi-planar C_{2v} B_{36}^+ (**1**), forming the most stable product C_s $B_{36}CO^+$ (**1A**) in a barrier-free process (Fig. S7) with a chemisorption energy of 0.86 eV at DLPNO-CCSD(T). The first experimentally observed $B_{36}CO^+$ can thus be assigned to $B_{36}CO^+$ (**1A**). The second CO molecule favours to be coordinated to an adjacent tri-coordinate vertex site at the corner on the outer B_{18} ring next to the first CO, generating the high-symmetry C_{2v} $B_{36}(CO)_2^+$ (**2A**) in a barrier-free process with a chemisorption energy of 0.98 eV, as presented in Fig. 2(a) and Fig. S8. The TS1 between **1A** and **2A** has a negative energy barrier of −0.09 eV relative to the entrance channel ($B_{36}CO^+$ (**1A**) + CO) (Fig. S8(b)). The second CO can also be adsorbed barrier-free at the opposite tri-coordinate vertex site of the first CO ligand in a sub-chemisorption pathway (Fig. S8(a)), forming the slightly less favourable isomer C_{2v} $B_{36}(CO)_2^+$ (**2B**) with an adsorption energy of 0.86 eV at the same theoretical level. **2A** and **2B** are expected to coexist in the cluster beam, with the former as the major isomer. Similarly, the experimentally observed $B_{36}(CO)_3^+$ and $B_{36}(CO)_4^+$ can be assigned to the most favourable C_1 $B_{36}(CO)_3^+$ (**3A**) and C_{2v} $B_{36}(CO)_4^+$ (**4A**), which can be produced in barrier-free adsorption processes (Fig. S9 and S10), with chemisorption energies of 0.84 and 0.89 eV, respectively.

Interestingly, the adsorption of the fifth CO ligand to the high-symmetry C_{2v} $B_{36}(CO)_4^+$ (**4A**) to form C_s $B_{36}(CO)_5^+$ (**5A**) with a chemisorption energy of 0.60 eV encounters a small positive energy barrier of +0.05 eV at TS5 (Fig. 3(a) and Fig. S11), consistent with the observation that only a weak experimental signal was observed for $B_{36}(CO)_5^+$ in Fig. 1(e). The sixth CO is coordinated to C_s $B_{36}(CO)_5^+$ (**5A**) at the available tri-coordinate vertex site *via* a barrier-free process, with a negative energy barrier of −0.03 eV at TS6, generating C_s $B_{36}(CO)_6^+$ (**6A**) with a chemisorption energy of 0.81 eV (Fig. 2(a) and Fig. S12). In the most favourable adsorption pathway, all the six tri-coordinate vertex sites at the six corners of C_{2v} B_{36}^+ (**1**) are occupied by six CO ligands in C_s $B_{36}(CO)_6^+$ (**6A**). Further calculations in Fig. S13 indicate that the adsorption of one more CO to C_s $B_{36}(CO)_6^+$ (**6A**) at a tetra-coordinate B atom encounters a significant positive barrier of +0.15 eV at TS7, consistent with the experimental observation that no $B_{36}(CO)_7^+$ mass signal was detected even under extended reaction times or elevated CO pressures. The experimental and theoretical results obtained above clearly indicate that the six tri-coordinate vertex B atoms on the B_{18} outer ring in C_{2v} B_{36}^+ (**1**) are much more reactive towards CO than their tetra-coordinate neighbors both kinetically and thermodynamically.

The overall chemisorption pathway C_{2v} B_{36}^+ → C_s **1A** → C_{2v} **2A** → C_1 **3A** → C_{2v} **4A** → C_s **5A** → C_s **6A** presented in Fig. 3(a) releases a total chemisorption energy of E_c = 4.98 eV upon the successive adsorption of six CO ligands at DLPNO-CCSD(T) (Fig. 2(a)). As shown in Fig. 2(c), the chemisorption energy E_c with respect to reaction (2) exhibits an almost perfect linear relationship with the number of CO ligands (n) involved in chemisorption processes: $E_c = 0.83n + 0.09$, with an average chemisorption energy of 0.83 eV per CO, suggesting that the six CO ligands are consecutively coordinated to the six tri-coordinate vertex sites on the outer B_{18} ring almost independently, with no significant structural changes introduced into the B_{36}^+ framework ($[B_6©B_{12}©B_{18}]^+$). The average chemisorption energy of 0.83 eV per CO in $B_{36}(CO)_n^+$ (n = 1–6) appears to be obviously smaller than that in $B_{11}(CO)_n^+$ (n = 1–6, 0.98 eV) and $B_{15}(CO)_n^+$ (n = 1–5, 1.05eV) at the same theoretical level,[17] consistent with the observation discussed above that the quasi-planar B_{36}^+ is about 1000 times less reactive towards the first CO than B_{11}^+ and B_{15}^+ in kinetics.

Using the perfect bowl-shaped C_{6v} B_{36} (**2**) as the coordination center, the chemisorption pathways of neutral $B_{36}(CO)_n$ (n = 1–6)

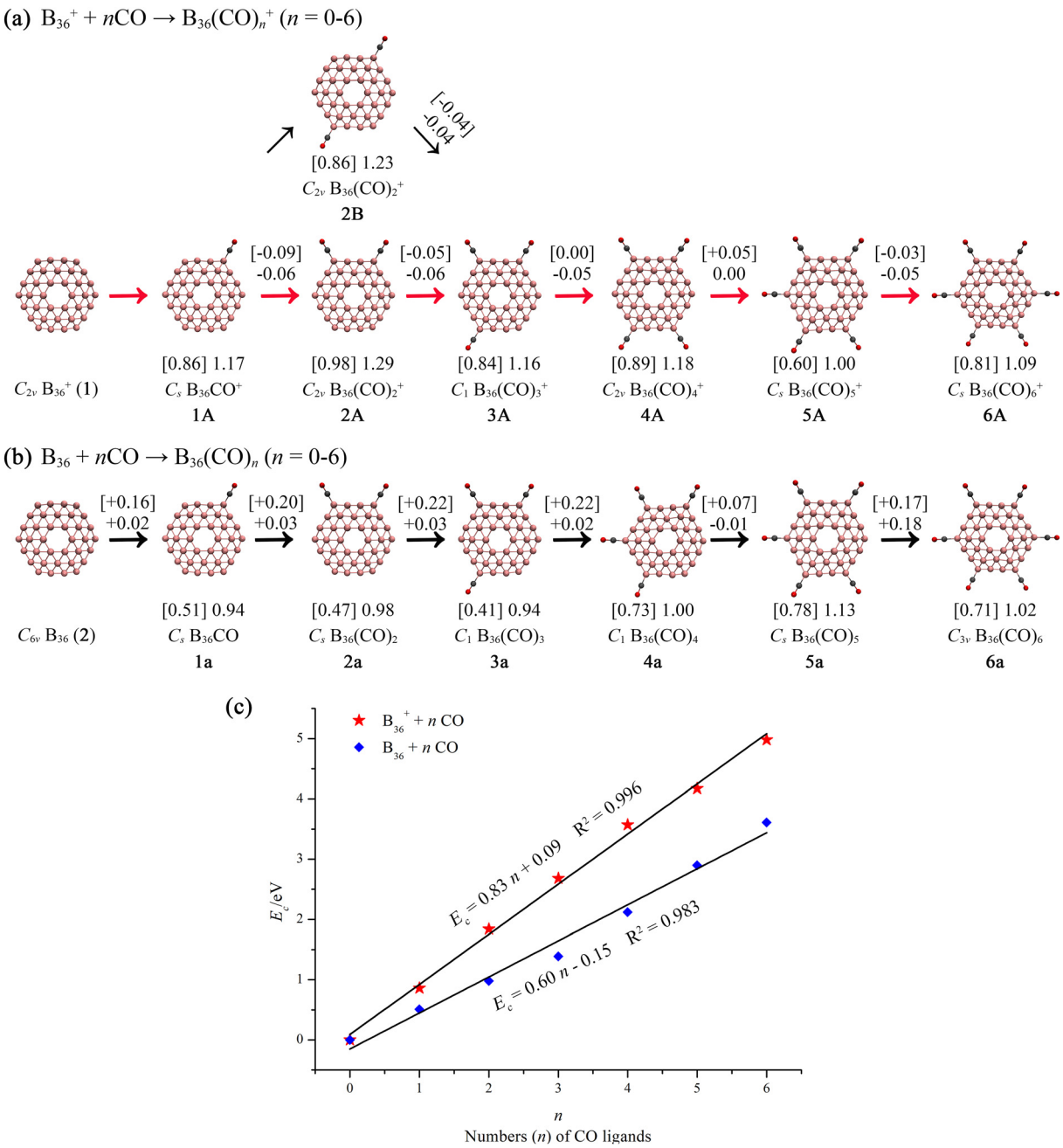

Fig. 2 Optimized structures and chemisorption pathways of (a) $B_{36}(CO)_n^{+}$ monocations (n = 1–6) and (b) $B_{36}(CO)_n$ neutrals (n = 1–6), with the chemisorption energies and corresponding energy barriers indicated in eV at DLPNO-CCSD(T)/cc-pvtz (in square brackets) and the PBE0-D3/6-311+G(d) levels. (c) Variations of the calculated chemisorption energies E_c with the numbers (n) of CO ligands in the concerned complexes with respect to $B_{36}^{+} + nCO \rightarrow B_{36}(CO)_n^{+}$ and $B_{36} + nCO \rightarrow B_{36}(CO)_n$ (n = 1–6), respectively.

were also optimized in Fig. 2(b) and Fig. S14–S19. With the significant positive energy barriers of +0.16, +0.20, +0.22, +0.22, +0.07, and +0.17 eV at TS8, TS9, TS10, TS11, TS12, and TS13 for n = 1, 2, 3, 4, 5, and 6 at DLPNO-CCSD(T), respectively, neutral $B_{36}(CO)_n$ (n = 1–6) are expected to be obviously less favourable in kinetics than their $B_{36}(CO)_n^{+}$ monocations. Fig. 2(c) shows that the chemisorption energies of neutral $B_{36}(CO)_n$ also follow an approximately linear relationship E_c = 0.60n −0.15 with the number of CO ligands, with the total chemisorption energy of E_c = 3.61 eV for n = 1–6 and average chemisorption energy of 0.60 eV per CO. The highly stable neutral C_{6v} B_{36} (**2**) is therefore obviously less reactive towards CO than its more electron-deficient monocation C_{2v} B_{36}^{+} (**1**) in both kinetics and thermodynamics.

Bonding pattern and aromaticity analyses

Detailed AdNDP bonding analyses were conducted on $B_{36}(CO)_n^{+}$ (n = 0–6) in Fig. S20–S22 to better comprehend their electronic and geometrical structures, with that of C_{2v} B_{36}^{+} (**1**),

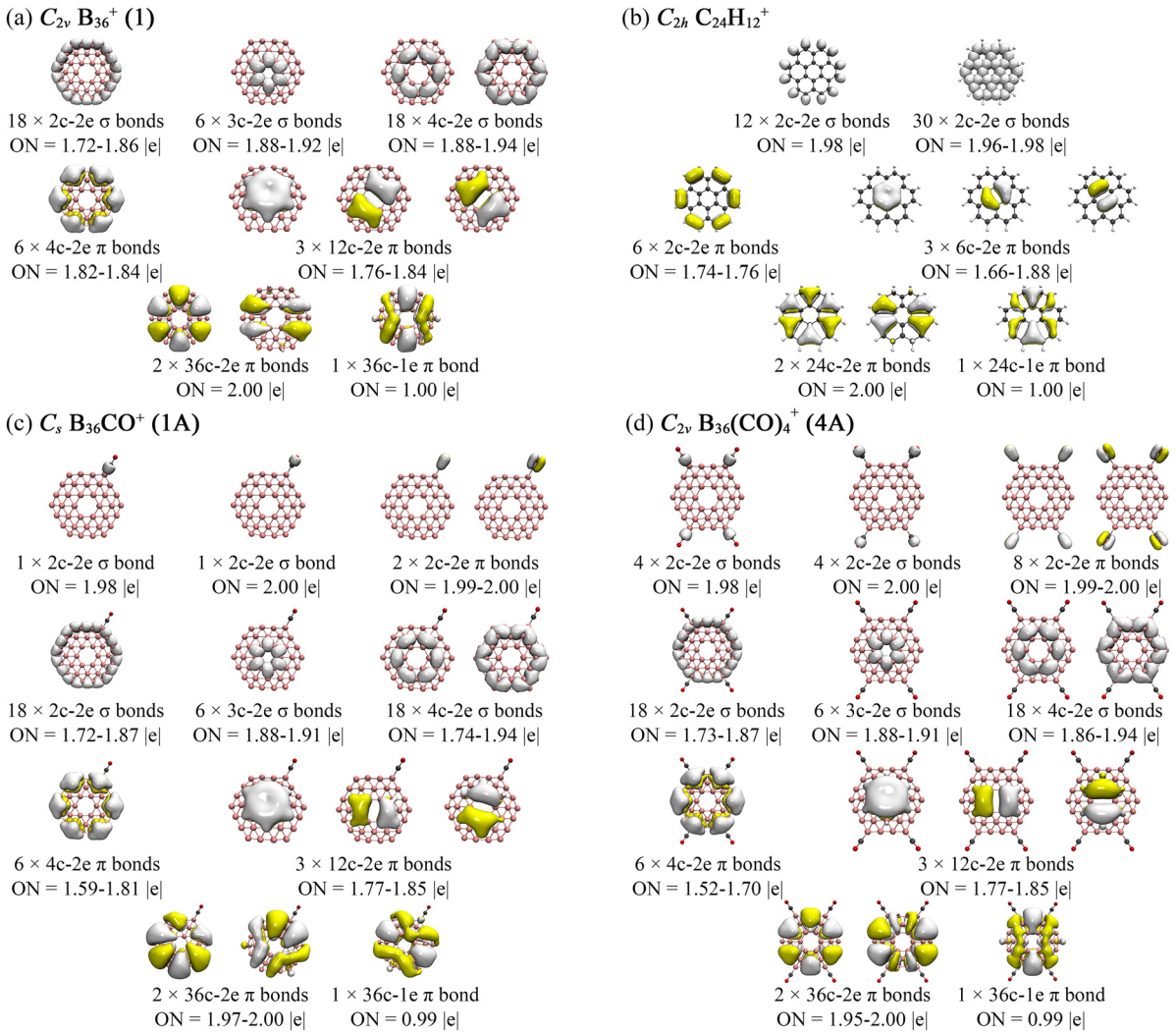

Fig. 3 AdNDP bonding patterns of (a) C_{2v} B_{36}^+(**1**), (c) C_s $B_{36}(CO)^+$ (**1A**), and (d) C_{2v} $B_{36}(CO)_4^+$ (**4A**) compared with that of coronene monocation (b) C_{2h} $C_{24}H_{12}^+$, with the occupation numbers (ONs) indicated and the σ-lone pairs on O atoms omitted.

C_{2h} $C_{24}H_{12}^+$, C_s $B_{36}(CO)^+$ (**1A**), and C_{2v} $B_{36}(CO)_4^+$ (**4A**) depicted in Fig. 3. The open-shell C_{2v} B_{36}^+ (**1**) possesses 18 2c–2e σ-bonds along the periphery of the outer B_{18} ring, 6 3c–2e σ-bonds and 6 4c–2e σ-bonds between the inner B_6 and middle B_{12} rings, and 12 4c–2e σ-bonds between the middle B_{12} and outer B_{18} rings. The remaining six bonds include 3 12c–2e π-bonds partially delocalized between the inner B_6 and middle B_{12} rings and 2 36c–2e π-bonds and 1 36c–1e π-bond totally delocalized over the whole B_{36} framework, forming a concentric 6π©5π system. As expected, with one more valence electron than C_{2v} B_{36}^+ (**1**), the closed-shell neutral C_{6v} B_{36} (**2**) possesses 3 12c–2e π-bonds partially delocalized between the inner B_6 and middle B_{12} ring and 3 36c–2e π-bonds totally delocalized over the whole B_{36} framework, forming a concentric 6π©6π system featuring concentric dual π-aromaticity.[20] Interestingly, as shown in Fig. 3c and d, the C_s $B_{36}(CO)^+$ (**1A**) and C_{2v} $B_{36}(CO)_4^+$ (**4A**) monocations well inherit the basic σ and π bonding patterns of C_{2v} B_{36}^+ (**1**) over the quasi-planar B_{36}^+ framework, with 1 2c–2e B_{36}^+-CO and 4 2c–2e B_{36}-CO σ-coordination bonds formed between the electron-deficient B_{36}^+ coordination center and electron-rich:C≡O σ-ligands, respectively. Similar bonding patterns exist in C_{2v} $B_{36}(CO)_2^+$ (**2A**), C_s $B_{36}(CO)_3^+$ (**3A**), C_s $B_{36}(CO)_5^+$ (**5A**), and C_s $B_{36}(CO)_6^+$ (**6A**), which form two, three, five, and six B_{36}^+-CO σ-coordination bonds, respectively (Fig. S20–S22). More remarkably, the π-bonding patterns of these $B_{36}(CO)_n^+$ boron carbonyl complexes (n = 1–6) closely resemble to that of coronene monocation C_{2h} $C_{24}H_{12}^+$ in Fig. 3b, with the 3 12c–2e, 2 36c–2e, and 1 36c–1e π-bonds in the former corresponding to the 3 6c–2e, 2 24c–2e, and 1 24c–1e π-bonds in the latter, respectively, presenting the first boron carbonyl monocations with two concentric delocalized π-systems analogous to that of coronene monocation $C_{24}H_{12}^+$ (6π©5π). As anticipated, $B_{36}(CO)_n$ neutral complexes (n = 1–6) with one more π-valence electron than $B_{36}(CO)_n^+$ possess two concentric π-systems (6π©6π) (Fig. S23–S25), forming a series of neutral boron carbonyl analogs of coronene $C_{24}H_{12}$.

The aromatic nature of the observed $B_{36}(CO)_n^+$ monocations is further evidenced by their calculated nucleus-independent

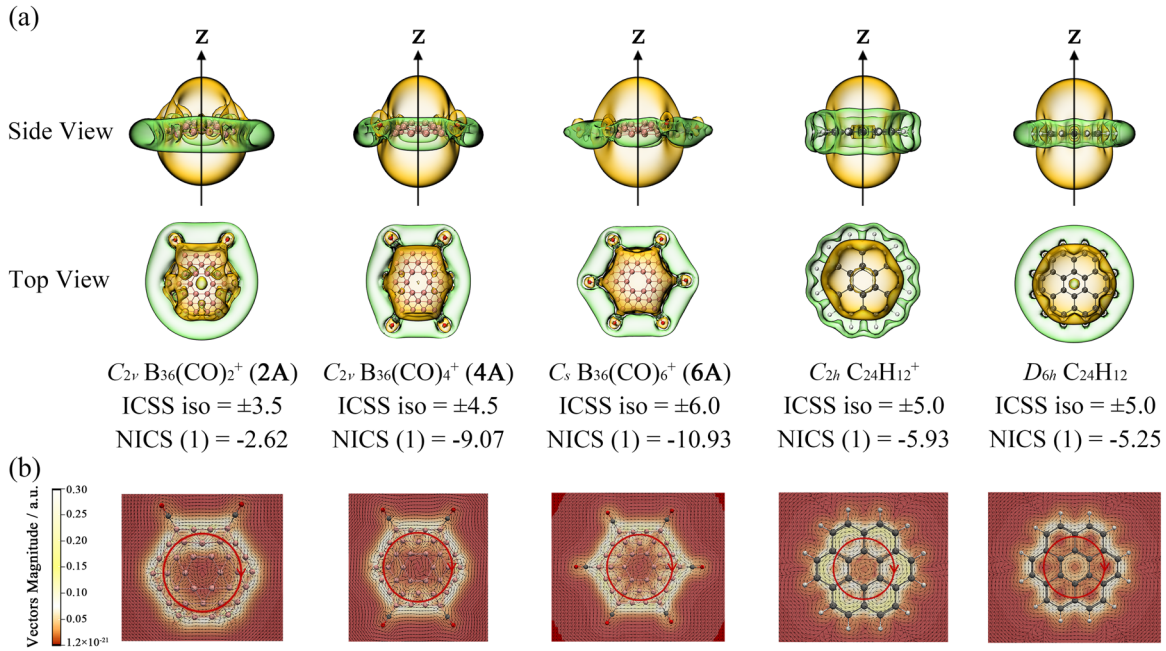

Fig. 4 (a) Calculated ICSS surfaces of C_{2v} $B_{36}(CO)_2^+$ (**2A**), C_s $B_{36}(CO)_4^+$ (**4A**), and C_s $B_{36}C_6O_6^+$ (**6A**), compared with that of C_{2h} $C_{24}H_{12}^+$ and D_{6h} $C_{24}H_{12}$, with the NICS(1) value 1.0 Å above the molecular planes indicated. (b) The corresponding calculated GIMIC plot 1.0 Å above the molecular planes, with the calculated ring current densities indicated in a.u. in the colour scale. The external magnetic field is perpendicular to the molecular plane. The red arrows denote the directions of the ring currents on the GIMIC iso-surfaces. Enlarged ICSS surfaces and GIMIC plots with higher resolutions are presented in Fig. S26–S29 for $B_{36}(CO)_n^+$ (n = 0–6), compared with that of neutral B_{36}.

chemical shift (NICS) values and GIMIC analyses. Based on the calculated NICS-ZZ components, Fig. 4(a) depicts the ICSSs of $B_{36}(CO)_n^+$ (n = 2, 4, 6), with the Z-axis perpendicular to the molecular planes, compared with that of coronene D_{6h} $C_{24}H_{12}$ and its monocation C_{2h} $C_{24}H_{12}^+$. C_{2v} $B_{36}(CO)_2^+$ (**2A**), C_{2v} $B_{36}(CO)_4^+$ (**4A**), C_s $B_{36}(CO)_4^+$ (**6A**), and C_{2h} $C_{24}H_{12}^+$ all appear to exhibit ICSS surfaces similar to that of the typical aromatic D_{6h} $C_{24}H_{12}$, where the spaces within about 1.0 Å above the molecular plane in vertical direction belong to chemical shielding regions highlighted in yellow with negative NICS-ZZ values, whereas the chemical de-shielding areas highlighted in green with positive NICS-ZZ values are located outside the quasi-planar B_{36} framework like a belt in the horizontal direction around the quasi-planar complexes. $B_{36}(CO)_2^+$ (**2A**), $B_{36}(CO)_4^+$ (**4A**), and $B_{36}(CO)_6^+$ (**6A**) possess the increasing negative calculated nuclear independent chemical shift values of NICS(1) = −2.62, −9.07, and −10.93 ppm 1.0 Å above the molecular planes, respectively, well comparable to the corresponding values of NICS(1) = −5.93 and −5.25 ppm in C_{2v} $C_{24}H_{12}^+$ and D_{6h} $C_{24}H_{12}$, indicating that these boron carbonyl monocations are all π-aromatic in nature.

GIMIC calculations revealed the magnetically induced ring currents 1.0 Å above the molecular planes of the concerned quasi-planar complexes. The calculated GIMIC clockwise current density vectors shown in Fig. 4(b) provide further evidence that the $B_{36}(CO)_n^+$ complexes and C_{2v} $C_{24}H_{12}^+$ with two concentric delocalized π-systems (6π + 5π) are all π-aromatic in nature, similar to the prototypical aromatic coronene D_{6h} $C_{24}H_{12}$, which possesses two concentric 6π + 6π systems. The calculated NICS(1) values and well-maintained robust current patterns in $B_{36}(CO)_n^+$ (n = 2, 4, 6) show that the carbonylation processes discussed above well preserve the aromatic character of the boron monocation.

Effective σ-donations and weak π-back-donations

To elucidate the coordination bonding patterns between the $B_{36}^{+/0}$ coordination center and CO ligands, detailed EDA-NOCV analyses were conducted on C_s $B_{36}CO^+$ (**1A**) monocation using B_{36}^+ and CO as interacting fragments in Fig. 5(a) and neutral C_s $B_{36}CO$ (**1a**) using B_{36} and CO as interacting fragments in Fig. 5(b), respectively, with the corresponding orbital interaction energies (ΔE_{orb}) and percentage contributions to overall interactions indicated. In C_s $B_{36}CO^+$ (**1A**), one dominant σ-donation from the HOMO of CO to HOMO-2 of B_{36}^+ contributes 59.72% to the total orbital interaction, whereas two weak π-back-donations from the HOMO−3 and HOMO−12 of B_{36}^+ to the two degenerate LUMOs of CO in two perpendicular directions contribute 18.73% and 8.84%, respectively. Similarly, the neutral C_s $B_{36}CO$ (**1a**) (Fig. 5b) exhibits one effective σ-donation contributing 55.21% and two weak π-back-donations contributing 21.26% and 9.22% to the overall orbital interaction, respectively. Such a coordination bonding pattern appears to be similar to that in classical transitional transition metal carbonyls (as exemplified by D_{3h} $Fe(CO)_5$ in Fig. S30) in which each CO ligand forms one effective σ-donation and two weak π-back-donations with the TM center, suggesting that the boron can be viewed as "honorary transition metals"

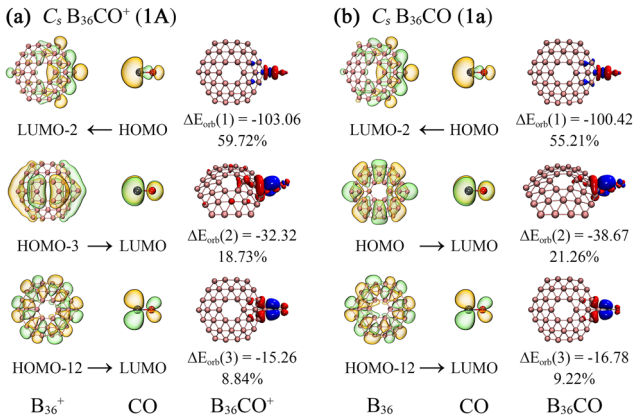

Fig. 5 Plots of the deformation densities $\Delta\rho$ and shapes of the most important interacting orbitals of the pairwise orbital interactions between (a) B_{36}^+ and CO in C_s $B_{36}CO^+$ (**1A**) and (b) B_{36} and CO in C_s $B_{36}CO$ (**1a**), with the orbital interaction energies ΔE_{orb} (in kcal mol^{-1}) and their percentage contributions to the overall orbital interactions indicated. The color code of the charge flow is from red to blue.

in $B_{36}(CO)_n^{+/0}$ complexes. A similar situation exists in the previously observed quasi-planar $B_{13}(CO)_n^+$ (n = 1–7)[16] with typical aromaticity and $B_{11}(CO)_n^+$ (n = 1–6) and $B_{15}(CO)_n^+$ (n = 1–5) with π and σ conflicting aromaticity.[17]

Conclusions

The joint experimental and theoretical investigations conducted in this study indicated that C_{2v} B_{36}^+ (**1**) as the well-defined global minimum of the monocation can chemisorb up to six CO molecules at the external vertices consecutively under ambient conditions to form a series of quasi-planar $B_{36}(CO)_n^+$ (n = 1–6) analogous to coronene monocation C_{2v} $C_{24}H_{12}^+$ in π-bonding, presenting the largest BCAs observed so far. It is the six tri-coordinate vertex B atoms at the six corners of C_{2v} B_{36}^+ (**1**) that define the maximum coordination number of n = 6 observed in $B_{36}(CO)_n^+$. B_{36}^+ (6π©5π) and B_{36} (6π©6π) with concentric dual π-aromaticity appear to be obviously less reactive towards CO than the previously reported B_{13}^+ (6π) with typical π-aromaticity, B_{11}^+ and B_{15}^+ with σ and π conflicting aromaticity, and B_{20}^+ with tubular aromaticity. There exist one effective σ-donation and two weak π-back-donations between each CO ligand and the B_{36}^+ coordination center in both $B_{36}(CO)_n^+$ and $B_{36}(CO)_n$ (n = 1–6) to help stabilize the complex systems, suggesting that boron as an amphotere element with partially occupied 2p orbitals can be viewed as an honorary transition metal in boron carbonyl complexes. With inspiration from the newly discovered nest-like C_1/C_s B_{56}^- ($[B_{12}@B_{44}]^-$), which can adsorb up to six C_2H_4, four CO, and one CO_2, further gas-phase chemisorption investigations on cage-like, bilayer, nest-like, and core–shell $B_n^{+/0/-}$ nanoclusters are currently in progress. Macroscopically synthesized boron carbonyl complexes are expected to have important potential applications in chemistry and materials science.

Conflicts of interest

There are no conflicts of interest to declare.

Data availability

All the data of this paper are available in the main text and supplementary information (SI). Supplementary information is available. See DOI: https://doi.org/10.1039/d5cp04719f.

Additional data can be obtained from the corresponding authors upon request.

Acknowledgements

This work was supported by the National Natural Science Foundation of China (Grant No. 22003034, 92461303, and 22373061).

References

1 X. Wu, L. Zhao, D. Jiang, I. Fernandez, R. Berger, M. F. Zhou and G. Frenking, *Angew. Chem., Int. Ed.*, 2018, **57**, 3974–3980.
2 W. A. Herrmann, *J. Organomet. Chem.*, 1990, **383**, 21.
3 J. B. Peng, H. Q. Geng and X. F. Wu, *Chemistry*, 2019, **5**, 526.
4 X. Wu, L. Zhao, J. Jin, S. Pan, W. Li, X. Jin, G. Wang, M. Zhou and G. Frenking, *Science*, 2018, **361**, 912.
5 A. B. Burg and H. I. Schlesinger, *J. Am. Chem. Soc.*, 1937, **59**, 780–787.
6 Y. M. Hamrick, R. J. Vanzee, J. T. Godbout, W. Weltner, W. J. Lauderdale, J. F. Stanton and R. J. Bartlett, *J. Phys. Chem.*, 1991, **95**, 2840–2844.
7 M. Zhou, N. Tsumori, Z. Li, K. Fan, L. Andrews and Q. Xu, *J. Am. Chem. Soc.*, 2002, **124**, 12936.
8 M. Zhou, Z. X. Wang, P. V. R. Schleyer and Q. Xu, *ChemPhysChem*, 2003, **4**, 763.
9 T. R. Burkholder and L. Andrews, *J. Phys. Chem.*, 1992, **96**, 10195.
10 M. Zhou, Q. Xu, Z. X. Wang and P. V. R. Schleyer, *J. Am. Chem. Soc.*, 2002, **124**, 14854.
11 Y. Zhao, T. Wang, C. Wang, Z. Zhang, H. Zheng, S. Jiang, W. Yan, H. Xie, G. Li, J. Yang, G. Wu, W. Zhang, D. Dai, X. Zheng, H. Fan, L. Jiang, X. Yang and M. Zhou, *ChemPhysChem*, 2022, **23**, e202200060.
12 J. Y. Jin, G. J. Wang and M. F. Zhou, *Chin. J. Chem. Phys.*, 2016, **29**, 47.
13 J. Jin, G. Wang and M. Zhou, *J. Phys. Chem. A*, 2018, **122**, 2688.
14 J. Jin, G. Wang, M. Zhou, D. M. Andrada, M. Hermann and G. Frenking, *Angew. Chem., Int. Ed.*, 2016, **55**, 2078.
15 J. Jin and M. Zhou, *Dalton Trans.*, 2018, **47**, 17192.
16 R. N. Yuan, J. J. Chen, Q. Chen, Q. W. Zhang, H. Niu, R. Wei, Z. H. Wei, X. N. Li and S. D. Li, *J. Am. Chem. Soc.*, 2024, **146**, 31464.

17 R. N. Yuan, Q. Chen, H. Niu, C. Y. Gao, X. N. Zhao, Y. B. Wu, S. G. He and S. D. Li, *Phys. Chem. Chem. Phys.*, 2025, **27**, 7279.
18 H. Niu, Q. Chen, R. N. Yuan, Q. W. Zhang and S. D. Li, *Phys. Chem. Chem. Phys.*, 2025, **27**, 17922.
19 Z. A. Piazza, H. S. Hu, W. L. Li, Y. F. Zhao, J. Li and L. S. Wang, *Nat. Commun.*, 2014, **5**, 3113.
20 Q. Chen, G. F. Wei, W. J. Tian, H. Bai, Z. P. Liu, H. J. Zhai and S. D. Li, *Phys. Chem. Chem. Phys.*, 2014, **16**, 18282.
21 X. N. Wu, B. Xu, J. H. Meng and S. G. He, *Int. J. Mass Spectrom.*, 2012, **310**, 57.
22 Z. Yuan, Y. X. Zhao, X. N. Li and S. G. He, *Int. J. Mass Spectrom.*, 2013, **354**, 105.
23 Q. Chen, H. W. Choi, G. F. Wei, D. Kahraman, R. N. Yuan, Q. W. Zhang, Q. Q. Yan, X. N. Zhao, C. Y. Gao, Y. Y. Ma, R. Wei, Y. Gui, Z. P. Liu, S. D. Li and L. S. Wang, *Proc. Natl. Acad. Sci. U. S. A.*, 2025, **122**, e2510702122.
24 R. A. J. O'Hair, *Chem. Commun.*, 2006, 1469.
25 L. D. Socaciu, J. Hagen, U. Heiz, T. M. Bernhardt, T. Leisner and L. Wöste, *Chem. Phys. Lett.*, 2001, **340**, 282.
26 Z. Yuan, Z. Y. Li, Z. X. Zhou, Q. Y. Liu, Y. X. Zhao and S. G. He, *J. Phys. Chem. C*, 2014, **118**, 14967.
27 Y. Zhao, X. Chen and J. Li, *Nano Res.*, 2017, **10**, 3407–3420.
28 M. J. Frisch, G. W. Trucks, H. B. Schlegel, G. E. Scuseria, M. A. Robb, J. R. Cheeseman, G. Scalmani, V. Barone, B. Mennucci, G. A. Petersson, *et al.*, *Gaussian 16, Revision C.01*, Gaussian, Inc., Wallingford, CT, USA, 2016.
29 S. Grimme, S. Ehrlich and L. Goerigk, *J. Comput.Chem.*, 2011, **32**, 1456.
30 C. Adamo and V. Barone, *J. Chem. Phys.*, 1999, **110**, 6158.
31 R. Krishnan, J. S. Binkley, R. Seeger and J. A. Pople, *J. Chem. Phys.*, 1980, **72**, 650.
32 Y. Guo, C. Riplinger, U. Becker, D. G. Liakos, Y. Minenkov, L. Cavallo and F. Neese, *J. Chem. Phys.*, 2018, **148**, 011101.
33 F. Neese, *WIREs Comput. Mol. Sci.*, 2022, **12**, e1606.
34 T. H. Dunning Jr., *J. Chem. Phys.*, 1989, **90**, 1007–1023.
35 R. A. Kendall, T. H. Dunning Jr. and R. J. Harrison, *J. Chem. Phys.*, 1992, **96**, 6796–6806.
36 E. Oger, N. R. M. Crawford, R. Kelting and P. Weis, *Angew. Chem., Int. Ed.*, 2007, **46**, 8503.
37 C. Gonzalez and H. B. Schlegel, *J. Chem. Phys.*, 1989, **90**, 2154.
38 C. Gonzalez and H. B. Schlegel, *J. Phys. Chem.*, 1990, **94**, 5523.
39 N. V. Tkachenko and A. I. Boldyrev, *Phys. Chem. Chem. Phys.*, 2019, **21**, 9590.
40 D. Y. Zubarev and A. I. Boldyrev, *Phys. Chem. Chem. Phys.*, 2008, **10**, 5207.
41 W. Humphrey, A. Dalke and K. Schulten, *J. Mol. Graph.*, 1996, **14**, 33.
42 T. Lu and F. Chen, *J. Comput. Chem.*, 2012, **33**, 580.
43 H. Fliegl, S. Taubert, O. Lehtonen and D. Sundholm, *Phys. Chem. Chem. Phys.*, 2011, **13**, 20500.
44 Kitware, Inc., 2021, ParaView, an Open-Source Data Analysis and Visualization Application, https://www.paraview.org.
45 T. Ziegler and A. Rauk, *Theor. Chim. Acta*, 1977, **46**, 1.
46 M. P. Mitoraj, A. Michalak and T. Ziegler, *J. Chem. Theory Comput.*, 2009, **5**, 962.
47 M. Mitoraj and A. Michalak, *Organometallics*, 2007, **26**, 6576.
48 G. T. E. Velde, F. M. Bickelhaupt, E. J. Baerends, C. F. Guerra, S. J. A. Van Gisbergen, J. G. Snijders and T. Ziegler, *J. Comput. Chem.*, 2001, **22**, 931.
49 E. VanLenthe, E. J. Baerends and J. G. Snijders, *J. Chem. Phys.*, 1993, **99**, 4597.